THE PERFORMANCE OF CHARGE-COUPLED DEVICES IN SIGNAL PROCESSING AT LOW SIGNAL LEVELS*

S.P. Emmons D.D. Buss

Texas Instruments Incorporated
Dallas, Texas 75222

ABSTRACT Experimental data are presented characterizing the noise sources in surface-channel CCDs fabricated by conventional single-level processing in P-type silicon. These data were obtained through noise spectrum measurements on the output of a continuously running CCD shift register. Quantitative comparisons are made with noise levels predicted by the results of spectral analyses also included in this paper. A model is then developed for characterizing CCD noise in analog signal-processing applications. Finally, using a simple input model, the dominant noise sources are referred to the input to provide the circuit designer with a single equivalent input noise voltage.

I. INTRODUCTION

Because CCDs are capable of carrying out signal-processing operations on sampled analog data with no necessity for analog-to-digital conversion, they are well suited to narrow-bandwidth transversal filtering and analog time-delay applications, with delays of several hundred milliseconds possible. Since transversal filtering is often used for the extraction of low-level signals from noise, it is appropriate, in addressing the limitations of CCDs in this application, to consider noise sources in CCDs.

It is the goal of this paper to identify the sources of noise in CCDs as they relate to the performance in signal-processing applications at low signal levels. Pursuant to this goal, a summary of all noise sources in CCDs is presented in Subsection II.A in which these noises are grouped into four general categories. An analysis follows in Subsection II.B which establishes the spectral content of each of these categories as it is modified by the charge-transfer efficiency of the shift register. Experimental data are presented in Section III characterizing the noise sources in surface-channel CCDs fabricated by conventional single-level processing in P-type silicon. These data were obtained through noise-spectrum measurements on the output of a continuously running CCD shift register. Quantitative comparisons are made with noise levels predicted in Section II.

A model is developed in Section IV for characterizing noise in the CCD transversal filter which is the fundamental building block of linear signal-processing systems.

Finally, a simple model for characterization of inputs in CCDs is presented in Section V. Using this model, the dominant sources of noise are referred to the CCD input to provide the circuit designer with a single equivalent noise voltage.

II. ANALYSIS OF NOISE SOURCES IN CHARGE-COUPLED DEVICES

A. ORIGINS OF CCD NOISE

A number of papers and presentations have appeared in the literature characterizing noise sources in CCDs.[1-4] For reasons that will be clear in the section on noise-power spectra, these noise sources are grouped into four general categories:

(1) Input noise, i.e., noise that is applied to the input and is attenuated by transfers through the entire device.

*This work was supported by the Naval Electronic Systems Command under Contract No. N00039-73-C-0013.

(2) Leakage current noise, i.e., noise that is continuously being added to a charge packet as it travels down the device.

(3) Fast-interface-state noise, i.e., noise which results from a variance in the amount of charge transferred each clock period.

(4) Output noise, i.e., noise introduced after all transfers; e.g., amplifier noise.

As is common in the literature, it is convenient to describe noise in CCDs as an uncertainity in the charge in a given charge packet.

1. Input Noise

This general category refers to the uncertainty in each charge packet in the shift register which was introduced simultaneously with the introduction of signal information. As such, this uncertainty existed before any transfers were performed. (It is analogous to "fat zero" noise in a CCD imager.) The model for this noise is critically dependent on the technique used for introducing the signal.[5] It has for some time been proposed[3] that input noise should be reducible to the kTC limit, where C is CCD capacitance. In fact, this has been shown to be true where C is the capacitance of an intermediate node at the input.[5]

Analytically, input noise may be expressed in terms of a random variable, Q_i, representing the quantity of charge to which the input capacitance (C_i) is set. The variance on the number of electrons is given by

$$\overline{\xi_i^2} = \frac{1}{q^2}\,\mathrm{Var}(Q_i) = \frac{1}{q^2}\,(kTC_i)\ \text{electrons}^2 \qquad (1)$$

where k is Boltzmann's constant, T is the absolute temperature, and q is the electronic charge. It may be shown that the standard deviation on the process may be reduced to

$$n_i = \sqrt{\overline{\xi^2}} \cong 400\sqrt{C_i\,(\mathrm{pF})}\ \text{electrons} \qquad (2)$$

2. Leakage Current Noise

This general category describes the effect of charge introduced uniformly along the shift register such that all such charges do not experience the same number of transfers before arriving at the output. In signal processing, it refers specifically to thermally generated minority carriers which are assumed to be uniformly generated and collected along the shift register. This type noise is exactly equivalent to the noise associated with optically generated carriers collected by a continuously running CCD shift register. This general category of noise is characterized by shot noise and is analytically expressed in terms of the random variable, N_ℓ, which describes the number of electrons introduced into a given charge packet at a given location

$$\overline{\xi_\ell^2} = \mathrm{Var}\,(N_\ell) = \overline{N}_\ell = \frac{1}{q}\,\overline{Q}_\ell\ \text{electron}^2 \qquad (3)$$

or equivalently

$$n_\ell = \sqrt{\mathrm{Var}\,(N_\ell)} = \sqrt{\overline{N}_\ell}\ \text{electrons} \qquad (4)$$

where $\overline{Q}_\ell$ is the expected value of the random variable, Q_ℓ, characterizing the charge-accumulation process. For the case of dark current characterized by a leakage current density, J_ℓ amps/cm^2,

$$\overline{Q}_\ell = A_{eff}\,J_\ell\,\tau\ \text{coulombs} \qquad (5)$$

where A_{eff} is the effective area over which the current is collected and τ is the corresponding integration time which, in the analysis to follow, is given by the reciprocal of the clock frequency, (i.e., $\tau = T_c = 1/f_c$).

3. Fast-Interface-State Noise

In a surface-channel device, each time a charge packet is transferred under a CCD electrode, it comes into equilibrium with the fast surface states at the semiconductor-insulator interface by filling these states up to an equilibrium level. During its subsequent transfer, an expected quantity of charge is re-emitted into the charge packet and is transferrred with it. There is, however, an uncertainty in that quantity which results in an uncertainty in charge in the transferred packet and, hence, a noise. Since the next packet must initially fill (or empty) the surface states to the equilibrium level, the expected charge added or subtracted from it is dependent on the charge subtracted or added to the previous packet. If a random variable is defined as the quantity of charge added to an arbitrary charge packet during a single stage transfer, this random variable has been shown[3] to have zero expected value and a variance given by

$$\overline{\xi^2} = pA_g\,k\,T\,N_{ss}\,\log_e(2)\ \text{electron}^2 \qquad (6)$$

where A_g is the CCD gate area, k is Boltzmann's constant, T is the absolute temperature, N_{ss} is the

surface state density, and p is the number of phases. In other words, a quantity of noise electrons, n_f, is introduced into a given packet each stage transfer given by

$$n_f = \sqrt{\overline{\xi^2}} = \sqrt{pA_g\ k\ T N_{ss}\ \log_e (2)} \text{ electrons} \quad (7)$$

In this case, however, the quantity of noise electrons added to the n^{th} packet is highly correlated with that added to the $(n-1)^{th}$ and $(n+1)^{th}$ packets.

4. Output (or Amplifier) Noise

A great deal has been written about techniques for sensing charge at the output of a CCD.[1-6] This paper relates to transversal filters, in which special techniques are used to nondistructively sense charge at distributed points along the shift register. Since a noise analysis of this technique follows in Section IV, attention will be limited here to the conventional floating-diffusion amplifier used in the experimental setup for noise data. A simplified model describes this amplifier as a capacitive node which is preset to a reference voltage before introduction of a CCD charge packet. As such, the uncertainty in charge after preset represents a noise source and is given by Equations 1 and 2 with subscript i change to o, where C_o is the capacitance of the CCD output node.

B. SPECTRA OF CCD NOISE

In this section, the spectra of the various types of noise which can occur in a CCD will be discussed and the effect of charge-transfer inefficiency on each spectrum will be calculated. The four types of spectra to be discussed are:

(1) Input noise. The spectrum of input noise is assumed to be white at the input but charge-transfer inefficiency introduces correlation among the various charge packets which alters the spectrum at the output. In the ideal case, input noise results from Johnson noise on the input impedance (kTC noise).

(2) Leakage-current noise. The spectrum of leakage-current noise differs from input noise in that all of the latter is introduced at the input while the former is introduced all along a continuously operating CCD. It results from shot noise on the thermally generated leakage current.

(3) Fast-interface-state noise. Fast-interface-state noise resembles leakage-current noise because it is introduced continuously as the charge packet transfers down the CCD. However, fast-interface-state noise is correlated even with perfect charge transfer efficiency whereas leakage-current noise is not.

(4) Output noise. Output noise is, of course, unmodified by CTE and is assumed to be white.

For the purposes of discussing these noise spectra, $\eta(nT_c)$ is defined as the number of noise charges at the CCD output in the n^{th} clock period. A random variable, η, whose autocovariance,[7] $Q_\eta(mT_c)$, is defined by

$$Q_\eta(mT_c) = \overline{\eta(nT_c)\ \eta[(n+m)\ T_c]} \quad (8)$$

has a spectrum defined by

$$S_\eta(z) = \sum_{m=-\infty}^{+\infty} Q_\eta\ (mT_c) z^{-m} \quad (9)$$

This spectrum can be viewed in the frequency domain by substituting the definition

$$Z^{-1} = \exp[-2\pi\ f/f_c] \quad (10)$$

where $f_c = 1/T_c$ is the clock frequency. The frequency spectrum, $S_\eta(f) \equiv 1/f_c\ S_\eta(Z)$, is related to the output noise, $\overline{\eta^2} \equiv Q_\eta(o)$, by the relation

$$\overline{\eta^2} = \int_{-f_c/2}^{+f_c/2} S_\eta(f)\ df \text{ electron}^2 \quad (11)$$

and the function $S_\eta(f)$ will be used to characterize the noise mechanisms discussed in the remainder of this section.

$S_\eta(f)$ can be related to the single-sided output-noise voltage spectrum, $S_V(f)$, as measured with a wave analyzer through the relation

$$S_V(f) = 2S_\eta(f)\ \frac{q^2}{C_o^2}\ g^2\ G(f) \quad (12)$$

where C_o is the capacitance of the CCD output node, g is the voltage gain of the amplifier, and q is the electronic charge. G(f) is a function which characterizes the output waveform. For example, if

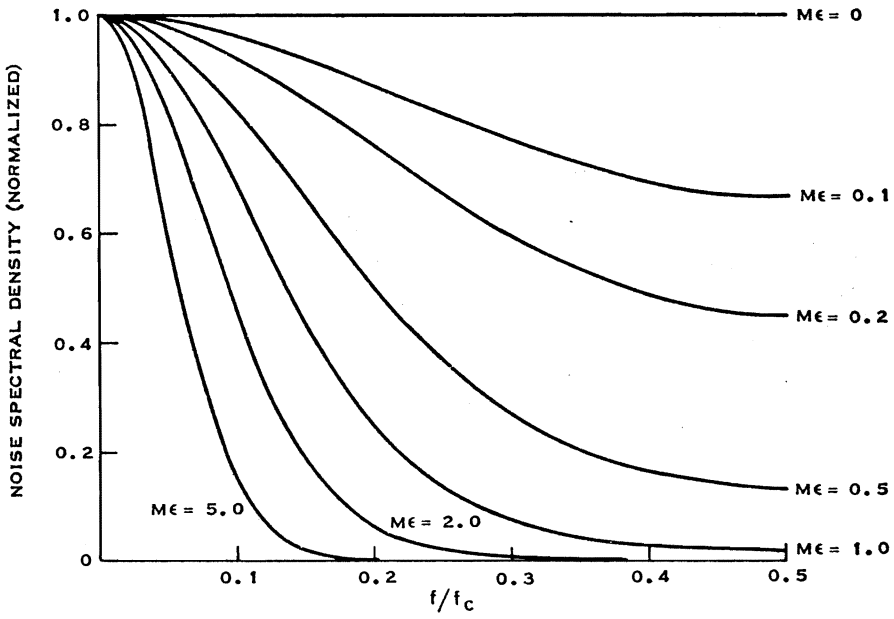

Figure 1. Normalized Power Density Spectrum of Input Noise as Modified by Charge Loss in CCD

the output voltage is sampled each period and held for a time $T_o \leq T_c$, then

$$G(f) = \left(\frac{T_o}{T_c}\right)^2 \frac{\sin(\pi f T_o)}{\pi f T_o} \qquad (13)$$

1. Input Noise

Consider a p-phase CCD having N gates and M = N/p clock periods or stages of delay. The loss per stage, ϵ, is then p times the loss per transfer, α (i.e., $\epsilon = p\alpha$). A CCD shift register having M stages and a loss per stage ϵ has transfer function[8,9]

$$H^{SR}(z) = z^{-M}\left(\frac{1-\epsilon}{1-\epsilon z^{-1}}\right)^M \qquad (14)$$

which can be well approximated by

$$H^{SR}(z) \cong z^{-M} \exp[-M\epsilon(1 - z^{-1})] \qquad (15)$$

Therefore, if the input noise is $\overline{\xi_i^2}$ per charge packet, the output noise spectrum

$$S_\eta^i(f) = \overline{\xi_i^2}\,|H^{SR}(f)|^2/f_c = \left(\frac{\overline{\xi_i^2}}{f_c}\right)\exp[-2M\,\epsilon(1 - \cos 2\pi f/f_c)] \qquad (16)$$

where $\overline{\xi_i^2}$ is given by Equation 1. This function is normalized by the quantity $\overline{\xi_i^2}/f_c$ and plotted in Figure 1 as a function of f/f_c for various values of $M\epsilon$. The normalized factor has the significance of being the variance in the number of noise charges introduced into each charge packet at the input divided by f_c and is identically equal to $1/f_c$ times the variance in the number of output charges when $\epsilon = 0$.

2. Leakage-Current Noise

Assume that at each stage a noise charge is introduced having variance $\overline{\xi_g^2}$ and that the noise charges so introduced are all statistically independent. Since the noise introduced at the k^{th} location

transfers through only M − K + 1 stages, the output noise spectrum is

$$S_\eta^\ell(f) = \sum_{k=1}^{M} \frac{\overline{\xi_\ell^2}}{f_c} \exp[-2(M-k+1)\epsilon(1-\cos 2\pi f/f_c)] \tag{17}$$

where $\overline{\xi_\ell^2}$ may be obtained using Equations 3, 4, and 5. The summation can be approximated by an integral to give

$$S_\eta^\ell(f) = \left(\frac{M\overline{\xi_\ell^2}}{f_c}\right) \frac{1-\exp[-2M\epsilon(1-\cos 2\pi f/f_c)]}{2M\epsilon(1-\cos 2\pi f/f_c)} \tag{18}$$

As before, this function is normalized by the output variance, when $\epsilon = 0$ divided by f_c and plotted in Figure 2. These results show less attenuation with charge-transfer inefficiency than do the results of Figure 1 because, on the average, leakage-current noise sees only half the total length of the shift register.

3. Fast-Interface-State Noise

Fast-interface-state noise results from fluctuations in the number of charge carriers emitted from the fast interface states during each transfer.[3] Because a positive fluctuation in the $(n-1)^{th}$ charge packet results in a high probability of an approximately equal negative fluctuation in the n^{th} charge packet, the output noise in succeeding time intervals is highly correlated.

When $\epsilon = 0$, the noise spectrum is

$$S_\eta^f(f) = \left(\frac{2M\overline{\xi_f^2}}{f_c}\right)(1-\cos 2\pi f/f_c) \tag{19}$$

where $\overline{\xi_f^2}$ is the variance in the number of noise charges which results from fast interface states during transfer through one stage (p transfers for a p-phase device), as given by Equation 6. The total variance at the output is found by integrating Equation 19 to give $2M\,\overline{\xi_f^2}$.

The effect of charge transfer inefficiency can be determined in a way which is analogous to Equation 17.

$$S_\eta^f(f) = \sum_{k=1}^{M} \frac{2\overline{\xi_f^2}}{f_c}(1-\cos 2\pi f/f_c) \times \exp[-2(M-k+1)\epsilon(1-\cos 2\pi f/f_c)] \tag{20}$$

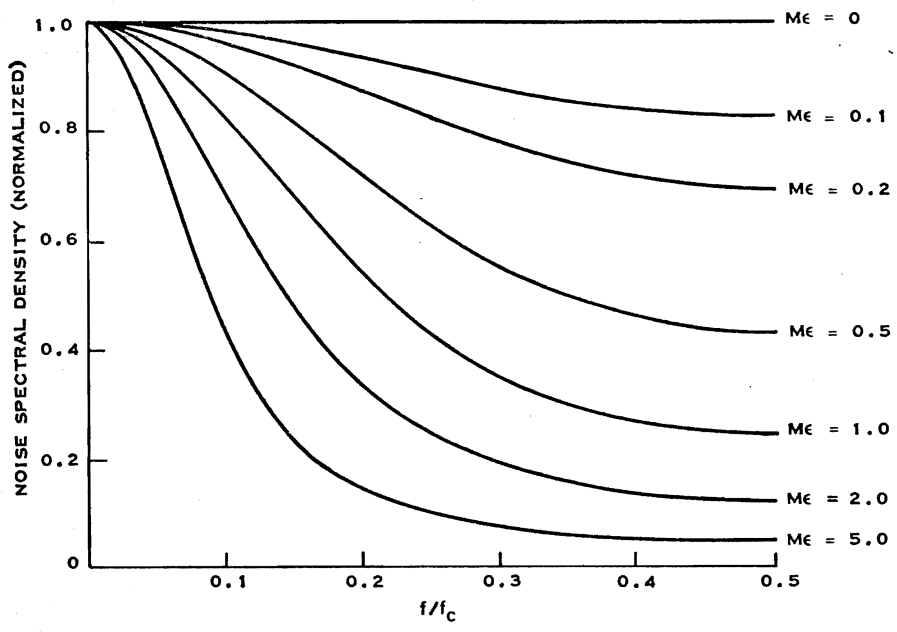

Figure 2. Normalized Power Density Spectrum of Leakage Noise as Modified by Charge Loss in CCD

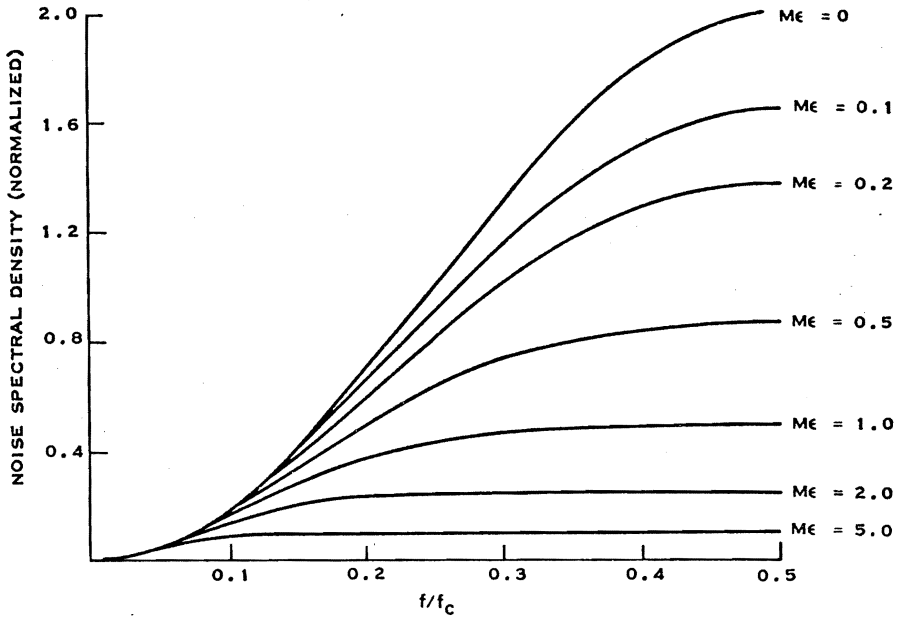

Figure 3. Normalized Power Density Spectrum of Surface-State Noise as Modified by Charge Loss in CCD

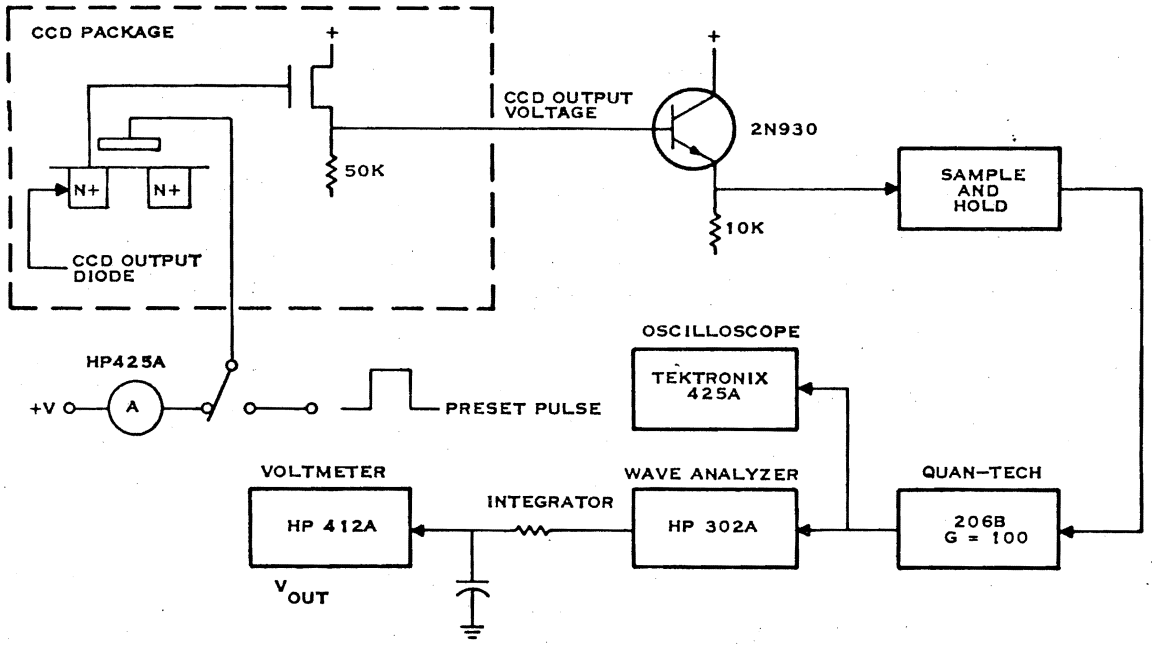

Figure 4. Spot Noise Measuring Equipment

Approximating the summation by an integral gives

$$S_\eta^{\,f}(f) = \left(\frac{2M\,\overline{\xi_f^2}}{f_c}\right) \frac{1 - \exp[-2M\epsilon(1 - \cos 2\pi f/f_c)]}{2M\epsilon} \qquad (21)$$

This function is normalized as in the previous cases and plotted in Figure 3. The normalized functions shown in Figure 3 are obtained from those of Figure 2 by multiplying by $[1 - \cos 2\pi f/f_c]$.

III. EXPERIMENTAL MEASUREMENT OF CCD NOISE

The experimental set-up used in these investigations is shown schematically in Figure 4. The output of a floating diffusion amplifier was decoupled first using a low-noise bipolar emitter-follower. An Analog Devices SHA-2 sample-and-hold amplifier was used to sample portions of the CCD output waveform. The noise bandwidth of the HP 302A wave analyzer was measured to be approximately 4 Hz. It is noted that provisions were made to connect the amplifier preset node to a dc voltage through a dc current meter (HP 425A) when the dc level of charge being transferred was to be determined. A HP 412A was connected to the wave analyzer recorder output through a long-time-constant integrator, as is common practice in noise measurements, to suppress fluctuations in the true RMS reading.

To facilitate the correlation of noise voltages measured by the wave-analyzer with the analyses in Section II, Equations 11 through 13 may be combined to yield

$$\overline{\eta^2} \equiv Q_\eta(o) = \frac{1}{R^2} \int_o^{f_c/2} \frac{S_v(f)}{G(f)}\, df \text{ electron}^2 \qquad (22)$$

where $\overline{\eta^2}$ is the variance on the random variable describing the charge in each packet arriving at the output. In Equation 22, R is the responsivity in volts/electron given by

$$R = \frac{q}{C_o}\, g \text{ volts/electron} \qquad (23)$$

where q is the electronic charge, C_o is the capacitance of the CCD output node (floating diffusion), and g is the voltage gain of the system between that node and the wave analyzer. As can be seen by inspection of Equation 13, for this case of near-100-percent-duty-cycle sample-and-hold operation ($T_o \cong T_c$), G(f) accounts for the (sin x/x) band-limiting effect of the sample-and-hold circuit.

It is readily seen by inspection of Equation 22 that, in the absence of band-limiting effects (i.e. G(f) = 1), the wide-band noise voltages over the Nyquist bandwidth ($f_c/2$) are numerically equal to the standard deviation $(\overline{\eta^2})^{1/2}$ on the number of electrons in the charge packet times the responsivity, R, of the system in volts/electron. Since both R and G(f) may be measured directly, Equation 22 allows the calculation of the uncertainty in charge in each packet from the noise spectrum measured by the wave analyzer. The theoretical spectral dependence of each of the types of noise sources are contained in Subsection II.B.

The continuously running shift register was selected as the optimum structure for obtaining quantitative measurements of the sources of noise in the CCD. Because of the availability of a monolithic precharge (floating diffusion) amplifier on a 64 X 64 area imager, initial data were taken on the output shift register of that device. The shift register had unusually poor CTE. The resulting high Mϵ product, however, provided useful information that the so-called transfer noise model[3] is not a valid source of noise in CCDs (at least for the transfer mechanisms present in these devices). This model is not discussed in this paper.

A typical waveform for the floating-diffusion amplifier on the output shift register of the 64 X 64 area imager is shown in Figure 5. The amplifier is shown schematically in Figure 6. The slight decrease in output voltage level (Figure 5) coincident with the collapse of the present pulse is caused by capacitive feedthrough. The large decrease in voltage level reflects the transfer of electrons onto the floating diffusion from the last potential well of the CCD. By monitoring the dc current being transferred by the CCD (see Figure 4), it was established that the responsivity of the amplifier was typically 1.8×10^{-6} volt per electron. The gain of the source follower with the 50K source resistor was measured to be approximately 0.8 from which the floating diffusion node capacitance was calculated to be approximately 0.07 pF.

Figure 7 shows how the SHA-2 sample-and-hold amplifier may be used to isolate amplifier noise from other CCD noise. Noise spectra may then be measured for both amplifier and CCD using the experimental setup of Figure 4.

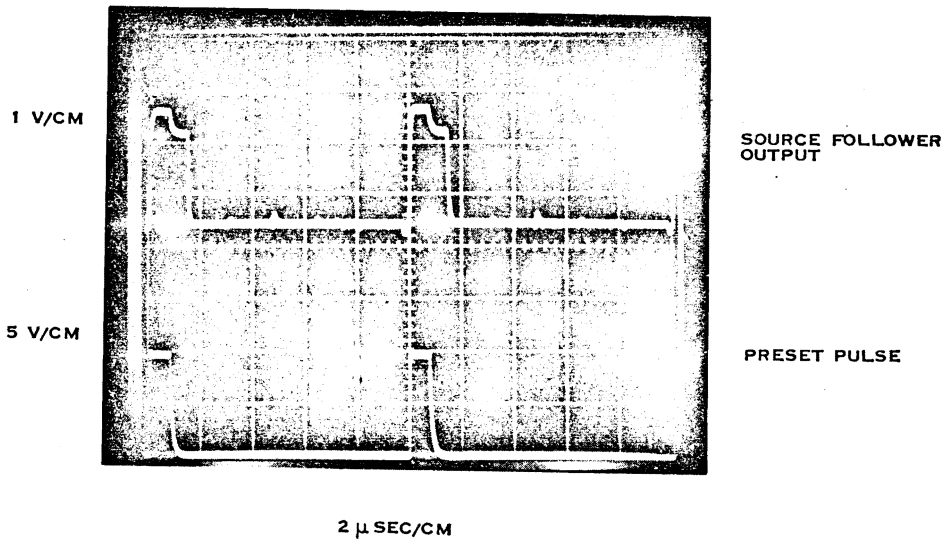

Figure 5. Typical Output Waveform of Floating-Diffusion Amplifier on 64 X 64 Imager

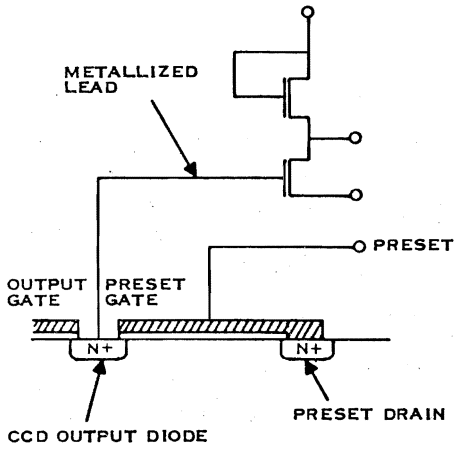

Figure 6. Schematic of Precharge Amplifier on 64 X 64 Imager

Using the noise spectra models of Section II, a theoretical prediction of the wave analyzer output was made for cases of both electrical and optical inputs to the CCD. The responsivity, R, defined in Equation 23 is the product of the 1.8×10^{-6} volt electron (measured for the preset amplifier) and the gain of 100 of the Quan-Tech 206B (see Figure 4). The noise bandwidth, B, of the HP 302A was measured to be 4 Hz. The expression for spectral noise power given by Equation 12 may be multiplied by B to obtain the noise power within the bandpass of the wave analyzer.* The clock frequency used for this experiment was 100 kHz at which CTE was measured by pulse techniques to be 0.993. The predicted spectrums of the noise voltages are shown in Figure 8. Since the amplifier noise may be sampled separately by the sample-and-hold technique, it is shown as a solid line. Also shown is the predicted output for an electrical input of arbitrary amplitude with its input noise added in quadrature with the predicted fast-interface-state noise and the amplifier noise. The predicted output in the absence of fast-interface-state noise is shown as a dashed line as is the predicted fast-interface-state noise. For comparison, the output of a leakage-current-type input (shot noise) was calculated for a condition producing a near full well of 1.25×10^6 electrons at the output. This is also shown in Figure 8.

The decrease in predicted amplifier noise at the high frequencies is caused by the sin x/x attenuation, G(f), introduced by the sample-and-hold. For the case

*This approximation is valid to the extent that the noise power is essentially constant over the narrow frequency range, B.

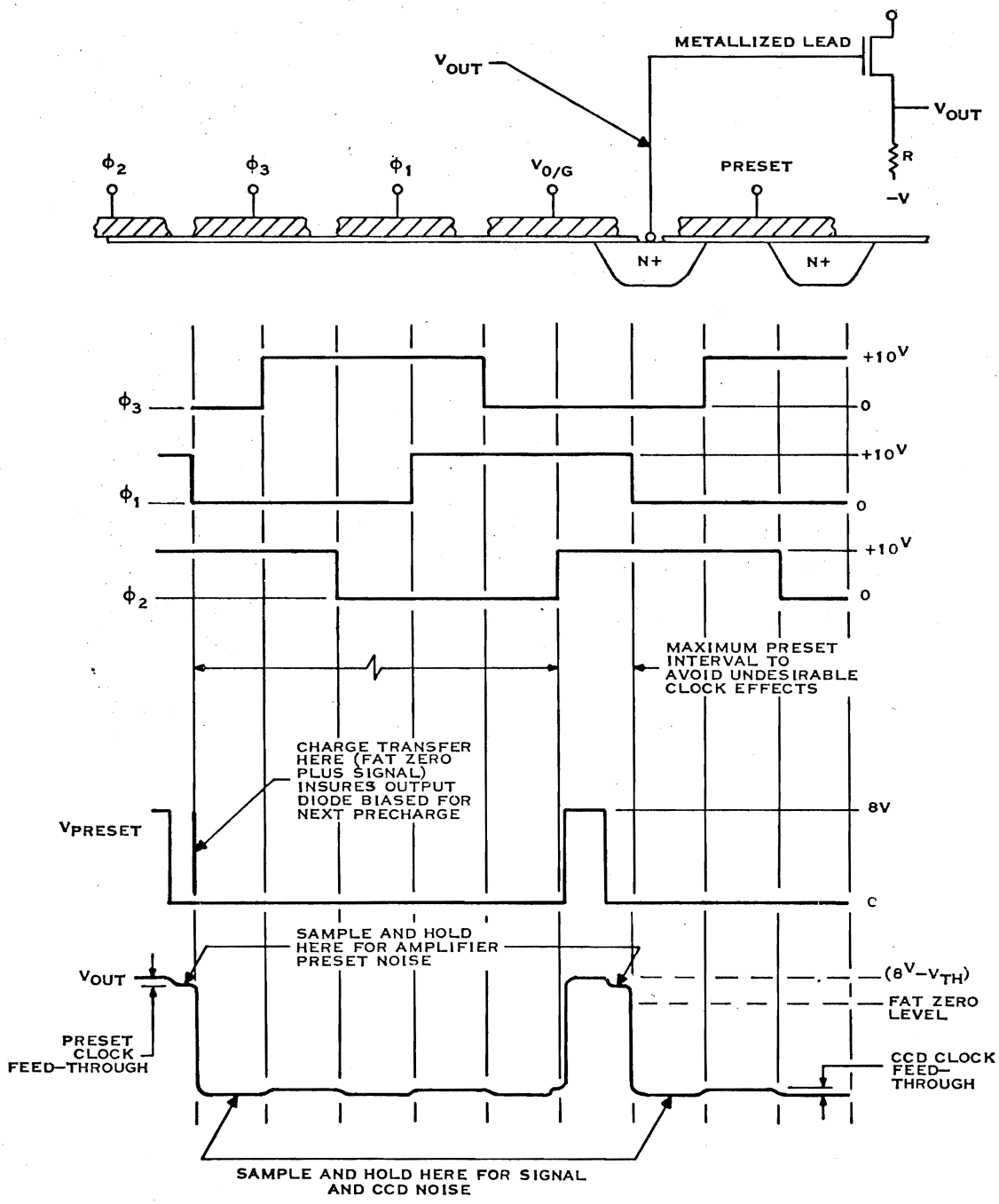

Figure 7. Schematic and Clocking Diagrams Describing Operation of Preamplifier on 64 X64 Imager

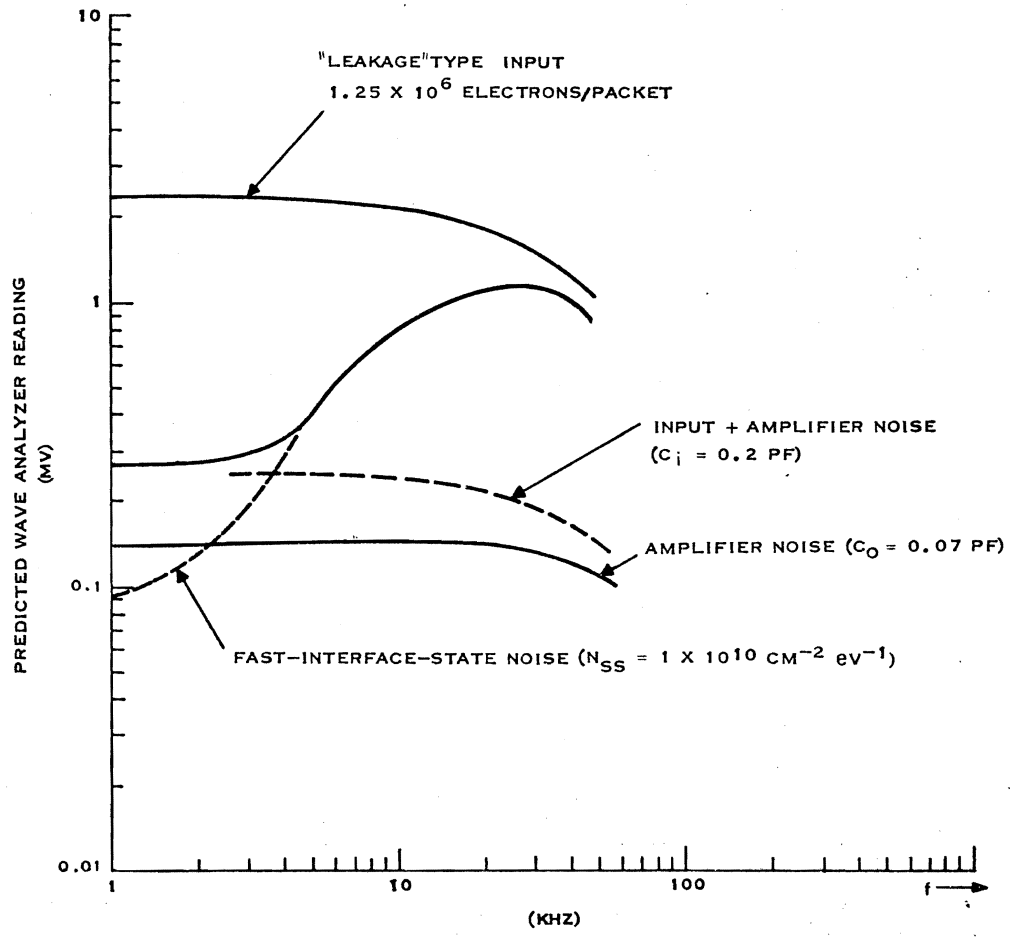

Figure 8. Predicted Noise Voltage Spectrum

of $G(f) \equiv 1$, amplifier noise would appear completely white (i.e., constant with frequency). Note that the correlated nature of the fast-interface-state noise causes it to peak at the high frequencies but to fall below that of both input noise and amplifier noise at the low frequencies. The leakage-current curve is that predicted for a uniform thermally or optically generated input resulting in an output level of 1.25×10^6 electrons per packet. Note that the dashed curve predicted as the output noise with an electrical input excluding fast-interface-state noise (but including amplifier noise) is valid for arbitrary input levels including a large level of 1.25×10^6 electrons/packet. This is a very important prediction in that it reflects the fact that the noise associated with large electrically-introduced signals is significantly less than full shot noise. (In the case of imagers, this model is relevant to so-called fat-zero noise.)

Data was taken for both electrical and optical (leakage-type) inputs. At these frequencies and temperatures, thermally-generated leakage-current noise is too low to measure in the presence of the other sources. To demonstrate that leakage-current noise is properly modeled by shot noise (and for obvious information relating to imaging application), the shift register was uniformly illuminated with visible light of sufficient intensity to produce an output current the dc value of which was measured to be 20 nA. At the 100 kHz clock frequency, this corresponded to 1.25×10^6 electrons per charge packet.

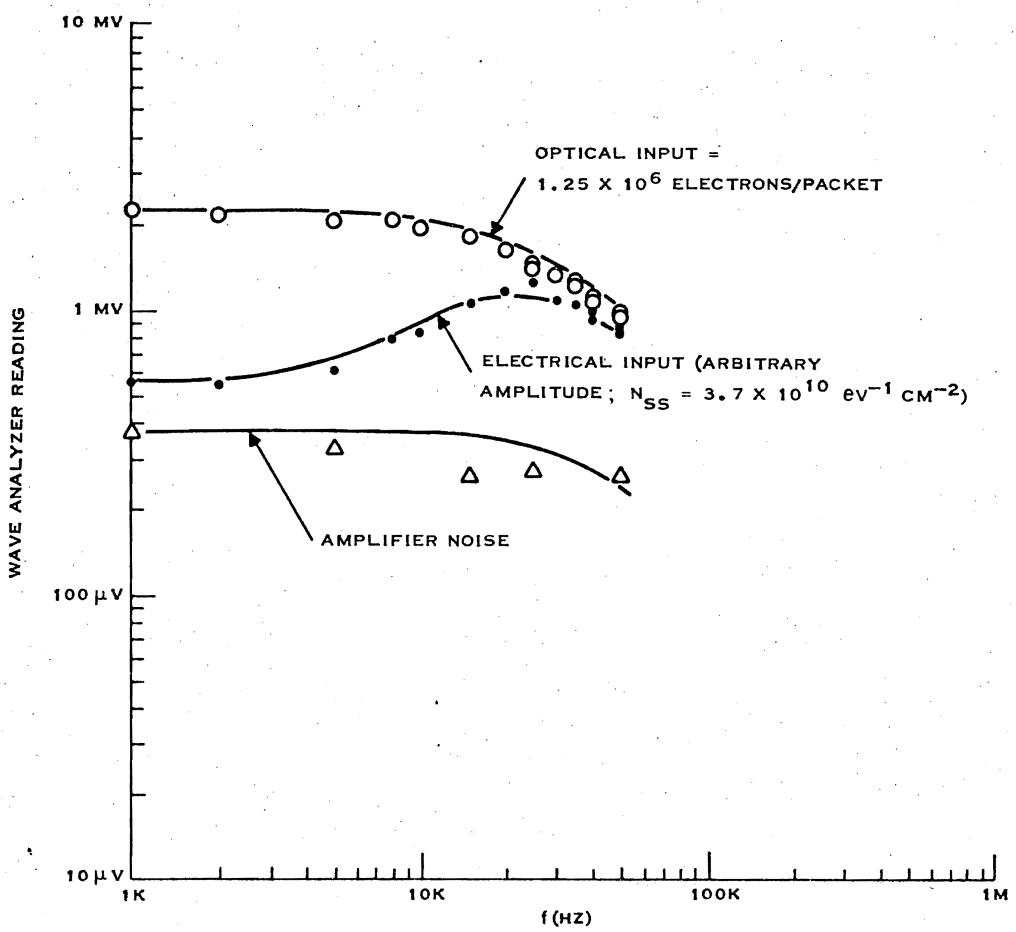

Figure 9. Theoretical and Experimental Spectral Output Noise After S and H

Electrical inputs of different levels were introduced including a level producing 1.25×10^6 electrons per packet. The results of these data are shown in Figure 9.

Comparison of Figure 9 to Figure 8 shows that data taken on this device indicated that both input noise and amplifier noise was significantly higher than that predicted. By adjusting the assumed variances on the charge levels for both amplifier and input noise as well as the interface-state density, N_{ss}, a fit with the data was obtained as shown in Figure 9. The solid lines are those predicted by the computer where the standard deviation on the input charge was assumed to be 220 electrons and the amplifier noise was taken to be 190 electrons rms. The surface fast-interface-state density was taken to be 3.7×10^{10} $(eV\text{-}cm^2)^{-1}$. The input and amplifier noise levels as measured were approximately twice those predicted by models for kTC type noise. Some of this excess noise was traced to the sample-and-hold circuits. Other possible sources of excess noise have since been identified and a technique developed in which the kTC limit has been essentially achieved for both amplifier and electrical input noise.[5] The data here, however, demonstrate the important fact that input noise need not be modeled by shot noise.

Reference to Figure 9 shows that the essential information describing the wideband noise per packet of all white-noise sources may be obtained by measuring the spot noise at a low enough frequency,

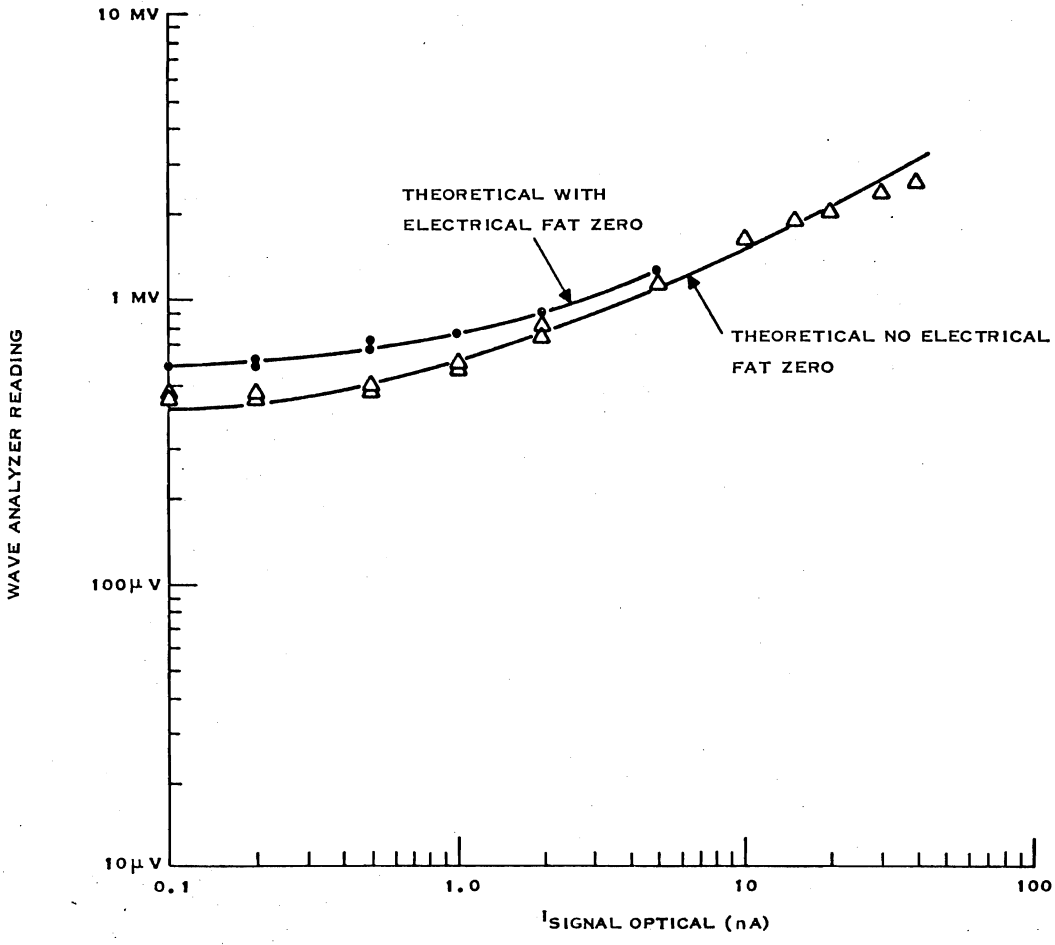

Figure 10. Theoretical and Experimental Output Noise After S and H

perhaps 1 kHz for f_c = 100 kHz, where sin x/x and MTF effects are negligible. Only the correlated fast-interface-state noise requires a spectral plot for complete characterization.

With this realization, subsequent data were taken. Spot noise was taken for different conditions only at 1 kHz. From these data, wideband white noise was obtained by multiplying the measured value by the square root of the ratio of the Nyquist frequency to the 4 Hz bandwidth of the wave analyzer. Equation 22 can then be used to calculate the variance in charge for the corresponding packet. A representative set of data on the same device as in Figure 9 is shown in Figure 10. The solid lines are the predicted values based on the same numbers that produced the fit in Figure 9. It is seen that the omission of the electrical input (fat zero) allowed slightly lower leakage-current (photon noise) levels to be detected. Again, the solid lines were those predicted by the analyses of Section II.

IV. NOISE IN CCD TRANSVERSAL FILTERS

In this section, how the various sources of noise discussed in the previous sections manifest themselves when a transversal filter is made with a CCD is discussed briefly.

As a review, a block diagram of a transversal filter is shown in Figure 11. It consists of a sampling stage, S, followed by M delay stages, D, each of which delays the signal by a time equal to a clock period, T_c. The signal is nondestructively sampled at each delay stage and then multiplied by the appropriate weighting coefficient, h_k (k = 1, M), and the weighted signals are summed together to give the filter output.

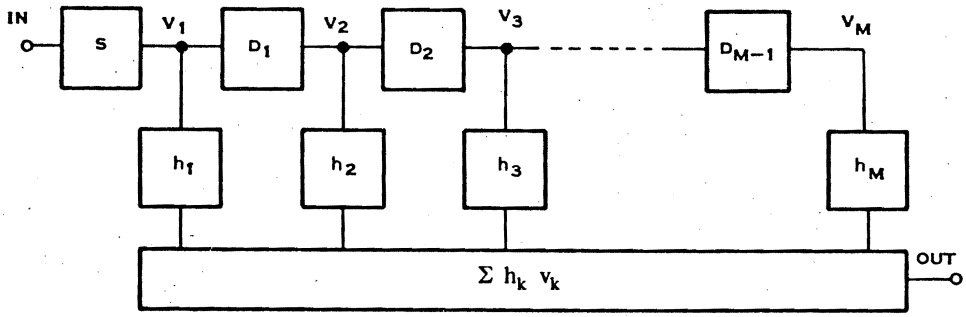

Figure 11. Transversal Filter Block Diagram

As can be seen from Figure 11, the h_k determines the impulse response, or Green's function, of the filter, i.e., the output which results when a single sample of unit amplitude is applied to the input. Moreover, when an arbitrary signal $v_{in}(t)$ is applied to the filter, the filter output is[9,10]

$$v_{out}(nT_c) = \sum_{k=1}^{M} h_k\ v_{in}(nT_c - kT_c) \qquad (24)$$

$$\approx \int_0^{T_d} h(\tau)\ v_{in}(nT_c - \tau)\ d\tau \qquad (25)$$

where $v_{in}(kT_c)$, represents the sampled input signal, and $T_d (= MT_c)$ is the total time delay of the filter. This output is approximately equal to the convolution of the input signal with the impulse response of the filter.

In constructing a transversal filter, it is necessary to have, in addition to an analog time delay, a circuit for sampling, weighting, and summing the outputs, as shown in Figure 11 and Equation 24. The technique described below was developed at Texas Instruments and has been used successfully in a number of CCD transversal filters which have been operated up to 5 MHz.

The principle used to nondestructively measure the charge under a CCD electrode is to integrate the current which flows in the clock line during charge transfer. For a three-phase (3-ϕ) CCD, when a transferred charge, Q_k^t, flows from under the k^{th} ϕ_2 electrode to under the k^{th} ϕ_3 electrode, the current that flows in the k^{th} ϕ_3 clock line can be separated into two portions: a portion that would flow if Q_k^t were zero, plus a portion that is approximately proportional to Q_k^t.

In a transversal filter, therefore, the output signal voltage, $V_{out}(nT_c)$, is a linear combination of the node voltages, v_k, as indicated by Equation 24. A number of noise electrons $\chi(nT_c)$ can be defined in a similar way by writing

$$\chi(nT_c) = \sum_{k=1}^{M} h_k\ \eta_k\ (nT_c) \qquad (26)$$

where $\eta_k(nT_c)$ is the number of noise electrons at the k^{th} node during the n^{th} clock period.

In the interest of clarity, neglect charge-transfer inefficiency ($\epsilon = 0$) for the analysis of this section. It can be included by combining the results of Subsection II.B with the present section. An ideal transversal filter has transfer function[7]

$$H(z) = \sum_{k=1}^{M} h_k\ z^{-k} \qquad (27)$$

The effects of each of the three types of noise considered in Subsection II.B will be calculated in terms of H(z) or H(f) which is obtained by using the definition of Equation 10.

A. INPUT NOISE

Using the definitions of Subsection II.B, together with Equation 26, autocovariance, $Q_\chi^i(mT_c)$, can be calculated for input noise. The result is

$$Q_x^i(mT_c) = \overline{\xi_i^2} \sum_{k=1}^{M-|m|} h_k\, h_{k+|m|} \qquad (28)$$

and this has transform

$$S_x^i(f) = \frac{\overline{\xi_i^2}}{f_c} |H(f)|^2 \qquad (29)$$

This is the expected result for a linear filter having input noise spectrum $\overline{\xi_i^2}/f_c$ and transfer function H(f). It will now be used to demonstrate how a transversal filter reduces noise by adding noise voltages incoherently while adding signal voltages coherently.

Consider an input signal having a number of electrons

$$n_s(k) = n_s\, g_k \qquad (30)$$

The g_k, like the h_k, is normalized so that $|g_k| \leq 1$. The input signal-to-noise ratio (SNR) is, therefore,

$$\text{SNR (in)} = \frac{n_s^2\, \overline{g^2}}{\overline{\xi_i^2}} \qquad (31)$$

The output signal is

$$N_s(nT_c) = n_s \sum_{k=1}^{M} h_k\, g_{n-k+1} \qquad (32)$$

and an important special case occurs when $g_k = h_{M-k+1}$, i.e., when the filter is matched to the input signal. (Even if the filter is not exactly matched as in bandpass filters, the above arguments approximately hold.) In this case,

$$\left[N_s(nT_c)\right]^2 = \frac{n_s^2}{f_c^2}\left[\int_{-f_c/2}^{+f_c/2} |H(f)|^2\, df\right]^2 \qquad (33)$$

and taking the ratio of Equation 33 to the integral of Equation 29 gives the output SNR

$$\text{SNR(out)} = \frac{n_s^2}{f_c\, \overline{\xi_i^2}} \int_{-f_c/2}^{+f_c/2} |H(f)|^2\, df \qquad (34)$$

Comparison of Equations 31 and 34 indicates that the signal-to-noise ratio at the output is greater than that at the input by a factor of M.

The foregoing discussion has shown how input noise can be reduced relative to the signal in a transversal filter. This type of noise reduction occurs when the signal is contaminated with noise before arriving at the filter[12] as well as when noise is added at the filter input. The way in which other types of CCD noise are reduced is similar but more complicated in detail.

B. LEAKAGE CURRENT NOISE

The autocovariance of leakage current noise is

$$Q_x^\ell(mT_c) = \overline{\xi_\ell^2} \sum_{k=1}^{M-|m|} k h_k\, h_{k+|m|} \qquad (35)$$

and this has spectrum

$$S_x^\ell(f) = \frac{i}{2\pi}\, \overline{\xi_\ell^2} \left(\frac{\partial H}{\partial f}\right) H^*(f) \qquad (36)$$

By setting $H(f) = \exp[-i2\pi\, Mf/f_c]$ in Equation 36, the result for an M-stage shift register is obtained.

Leakage-current noise is important in bandpass filtering at the low-frequency end of the sonar spectrum. A filter having a passband from 8 to 16 Hz requires a total storage time on the order of seconds. This is possible at room temperature because fixed-pattern leakage-current noise is not a factor and only the true shot noise considered in this paper limits filter performance. It is noted, however, that sources of 1/f noise have been neglected. Such sources in both input and output MOSFET structures may be very important for these low frequency applications.

C. FAST-INTERFACE-STATE NOISE

The calculation of the autocovariance of fast-interface-state noise is straightforward but tedious. The result is

$$Q_x^f(mT_c) = \overline{\xi_f^2}\left[2\sum_{k=1}^{M-|m|} kh_k\, h_{k+|m|} - \sum_{k=1}^{M-|m|-1} kh_k\, h_{k+|m|+1} - \sum_{k=1}^{M-|m|-1} kh_{k+1}\, h_{k+|m|}\right] \quad (37)$$

The transform of Equation 37 can be approximated by

$$S_x^f(f) = i\frac{\overline{\xi_f^2}}{\pi}\left(\frac{\partial H}{\partial f}\right) H^*(f)\left[1 - \cos 2\pi \frac{f}{f_c}\right] \quad (38)$$

Inspection of Equation 38, together with Equation 6 of Section II.A, shows that in some transversal filters, fast-interface-state noise dominates whereas in others it is negligible. In a lowpass filter, for example, fast-interface-state noise is largely eliminated because at low frequency the fast-interface-state noise spectrum is very small.

D. OUTPUT (OR AMPLIFIER) NOISE

Even if fast-interface-state noise can be eliminated with a buried-channel CCD, the noise performance of CCD transversal filters can not be substantially improved until techniques are developed to reduce output-amplifier noise. Improvements appear possible. However, the electrode-weighting technique[10] which has been most commonly used (See Figure 12) requires a differential current integrator (DCI) which operates on the principle of precharging two large capacitors, $C^{(+)}$ and $C^{(-)}$, which then charge the clock lines, $\phi_3^{(+)}$ and $\phi_3^{(-)}$. The DCI is therefore characterized by kTC noise on $C^{(\pm)}$ which must be large enough to charge the clock lines without appreciable loss of voltage.

A matched transversal filter discriminates against DCI noise just as it does other sources of CCD noise in the sense that the RMS DCI noise voltage increases only like $(M)^{1/2}$ whereas the signal voltage increases like M. For many practical filter designs, however, DCI noise dominates.

V. INPUT CONSIDERATION– EQUIVALENT INPUT NOISE VOLTAGE

Much has been written about the electrical introduction of charge into CCDs.[2,3,5] For the purpose of this paper, however, it suffices to state that all of the viable input schemes involve presetting a capacitive node (not necessarily the CCD potential well itself) to a voltage equal to (or displaced by a constant offset voltage from) the input voltage. The input schemes have the effect, then, of sampling the input voltage v_s periodically and producing a charge packet representing its sampled level. The RMS number of charges is given by

$$N_s = \frac{1}{q} Q_s = \frac{1}{q}(v_s\, C_i) \text{ electrons} \quad (39)$$

where C_i is the capacitance of the input node and v_s is the rms signal voltage. It was established in previous sections that a noise is associated with this sampling process given by Equations 1 and 2. Using Equation 39, all sources of noise in the CCD may be referred back to the CCD input in the form of an equivalent wideband RMS noise voltage, the spectral content of which is dependent on its source. For the sake of simplicity and to some extent justified practically, the effects of CTE will be neglected here and only the noise source considered to be dominant will be treated. As discussed in Section IV, with present technology in CCD transversal filters where M is not too large, the sample and weighting noise associated with presetting the large $C^{(\pm)}$ capacitors is dominant. For typical values of the capacitance, $C^{(\pm)}$, the output noise is calculated to be of the order of 1.2×10^3 RMS electrons. Neglecting CTE or MTF effects (as well as sin x/x effects) this noise charge is referred to the CCD input node. Equation 39 may now be used to transform this noise to an equivalent input wideband noise voltage. Since the kTC noise is assumed to be white, this noise voltage is also essentially white and equally distributed over the Nyquist bandwidth ($f_c/2$). It is an important observation that the input capacitance need not be equivalent to the capacitance of a single CCD potential well. Within limits, it is perfectly feasible to make this capacitance larger, in which case the equivalent input noise voltage predicted by Equation 29 is decreased. Table I shows the input noise voltage for several values of input node capacitance.

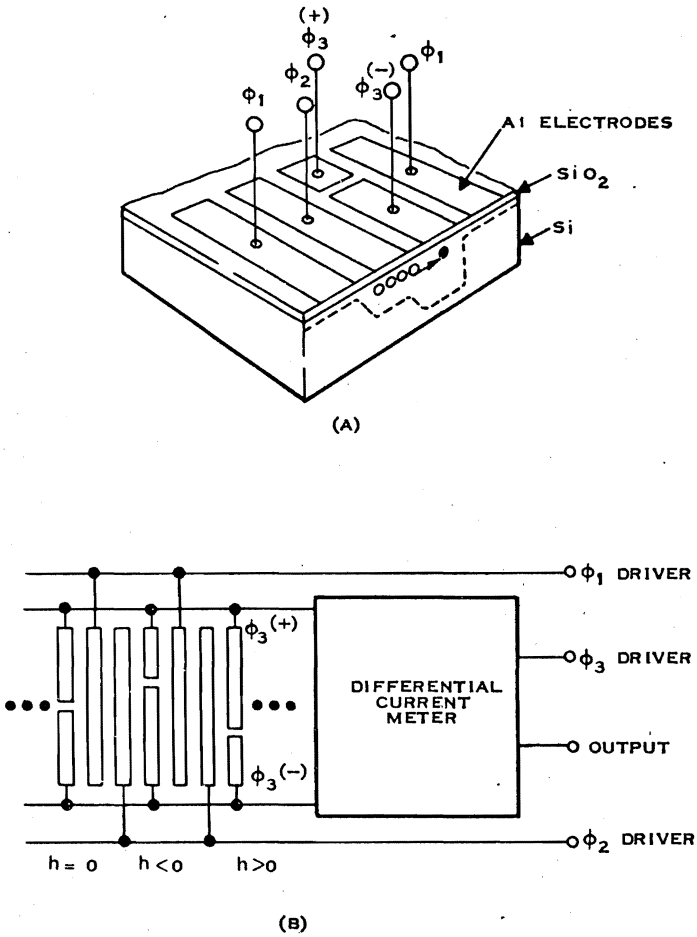

Figure 12. Schematic of Tapping and Summing Procedure Tested with CCD Filters

Table I. Equivalent Wideband Input Noise Voltage for CCD Transversal Filter Dominated by Output Sample and Weighting Noise (Typically 1.2×10^3 Electrons/Packet)

Input Node Capacitance (pF)	Input Noise Voltage (μV)
0.2	1,000
0.8	250
2.0	100

Dynamic Range ≅ 86 dB p-to-p signal/RMS noise (assumes 10 volts on phase clocks)

Table II. Equivalent Wideband Input Noise Voltage for 500 Stage CCD Transversal Filter with Noise Dominated by Fast Interface States*

Input Node Capacitance (pF)	Input Noise Voltage (μV)
0.2	2,200
0.8	550
2.0	220

Dynamic Range ≅ 80 dB p-to-p signal/RMS noise (assumes 10 volts on phase clocks)

*Using $N_{ss} = 2 \times 10^{10}$ cm^{-2} eV^{-1}, p = 3, and other parameters appropriate to a typical CCD structure and Equation 6.

Several factors, in addition to practical "real estate" considerations, limit the size of the input node capacitance. One is that the device used to preset the capacitance is usually a MOSFET which has an equivalent input noise voltage normally negligible when C_i is of the order of a CCD potential well. A second factor is that the input noise charge predicted by Equation 2 goes up as C_i is increased. A point may be theoretically reached when this noise charge becomes the dominant noise charge in the CCD, beyond which point the dynamic range of the CCD is decreased. Another consideration is the fact that the RC time associated with the MOSFET channel resistance–C_i combination may limit the speed of operation.

Table II shows a corresponding set of input noise levels for the case of M large where surface-state noise should be dominant. This table, of course, does not reflect the correlated nature of the fast-interface-state noise.

REFERENCES

1. G.F. Amelio, W.J. Bertram, and M.F. Tompsett, "Charge-Coupled Imaging Devices: Design Considerations," *IEEE Trans. on Electron Devices* ED-18, 11, 986, (1971).
2. D.F. Barbe, "The Charge-Coupled Concept," *Report of NRL Progress,* March 1972.
3. J.E. Carnes and W.F. Kosonocky, "Noise Sources in Charge-Coupled Device," *RCA Review,* Vol. 33, June 72 (327).
4. M.F. Tompsett, "The Qualitative Effects of Interface States on the Performance of CCD's," *IEEE Trans. on Electron Devices*, Vol. ED-20, No. 1, January 1973, pp. 45–55.
5. S.P. Emmons and D.D. Buss, "Techniques for Introducing a Low Noise Fat Zero in CCD's," 1973 Device Research Conference, Boulder, Colorado.
6. W.S. Boyle and G.E. Smith, "Charge-Coupled Semiconductor Devices," *Bell Sys. Tech. J.*, 49: 487 (1970).
7. B. Gold and C.M. Rader, *Digital Processing of Signals,* McGraw-Hill, 1969.
8. D.D. Buss, W.H. Bailey, and D.R. Collins, "Analysis and Applications of Analog CCD Circuits," Proceedings of 1973 IEEE International Symposium on Circuit Theory.
9. D.D. Buss and W.H. Bailey, "Applications of Charge Transfer Devices to Communication," 1973 CCD Applications Conference, San Diego, California.
10. D.D. Buss, D.R. Collins, W.H. Bailey, and C.R. Reeves, "Transversal Filtering Using Charge Transfer Devices," *IEEE J. Solid-State Circuits,* Vol. SC-8, No. 2, April 1973.
11. D.D. Buss, C.R. Reeves, W.H. Bailey, and D.R. Collins, "Charge Transfer Devices in Frequency Filtering," Proceedings of the 26th Annual Symposium on Frequency Control, 6-8 June 1972, pp. 171-179.
12. D.D. Buss and W.H. Bailey, "Spread Spectrum Communication Using Charge Transfer Devices, Proceedings of the 1973 Symposium on Spread Spectrum Communications, March 13-16, 1973.

REVERSE SIDE BLANK